Application of muon tomography to fuel cask monitoring

Poulson, Daniel Cris
Bacon, Jeffrey Darnell
Durham, J. Matthew
Guardincerri, Elena
Morris, Christopher
Trellue, Holly Renee

To be published in: Philosophical Transactions of the Royal Society A: Mathematical, Physical and Engineering Sciences

DOI to publisher's version: 10.1098/rsta.2018.0052

Permalink to record: http://permalink.lanl.gov/object/view?what=info:lanl-repo/lareport/LA-UR-18-24873

PHILOSOPHICAL TRANSACTIONS A

rsta.royalsocietypublishing.org

Research

Cite this article: Poulson D, Bacon J, Durham M, Guardincerri E, Morris CL, Trellue HR. 2019 Application of muon tomography to fuel cask monitoring. *Phil. Trans. R. Soc. A* **377**: 20180052. http://dx.doi.org/10.1098/rsta.2018.0052

Accepted: 4 October 2018

One contribution of 21 to a Theo Murphy meeting issue 'Cosmic-ray muography'.

Subject Areas:
particle physics, nuclear physics

Keywords:
muon, tomography, spent, fuel, cask

Author for correspondence:
C. L. Morris
e-mail: cmorris@lanl.gov

Electronic supplementary material is available online at https://dx.doi.org/10.6084/m9.figshare.c.4285733.

THE ROYAL SOCIETY PUBLISHING

Application of muon tomography to fuel cask monitoring

Dan Poulson, Jeff Bacon, Matt Durham, Elena Guardincerri, C. L. Morris and Holly R. Trellue

Los Alamos National Laboratory, Los Alamos, NM 87545, USA

EG, 0000-0002-7703-9988; CLM, 0000-0003-2141-0255

Long-term monitoring of spent fuel stored in dry cask storage is currently achieved through the use of seals and surveillance. Muon tomography can provide direct imaging that may be useful in cases where what is known as Continuity of Knowledge (CoK) has been lost using the former methods. Over the past several years, a team from Los Alamos National Laboratory has been studying the use of muon scattering and stopping to examine spent fuel in dry cask storage. Data taken on a partially loaded Westinghouse MC-10 fuel cask have demonstrated that muon scattering radiography can detect missing fuel assemblies. A model, validated by this data, shows that tomographic reconstructions of the fuel can be obtained in relatively short exposures. Model fitting algorithms have been developed for dealing with datasets with limited angular that appear to work well. Here we show that muon tomography can provide a fingerprint of a loaded fuel cask, because of its sensitivity to both the density and atomic charge of the spent fuel, and that it is sensitive to many diversion scenarios.

This article is part of the Theo Murphy meeting issue 'Cosmic-ray muography'.

1. Introduction

Nuclear reactors provide stable, electrical power with no carbon emissions. Although other renewable sources can compete in price, no other carbon-free sources can currently handle the base load to ensure a stable power distribution grid. The only currently viable path forward to zero carbon emission, stable power is replacing fossil fuel generation with nuclear power for the base load.

Several obstacles are blocking increased nuclear power production. These include the fact that there are few paths to the permanent safe storage of nuclear waste. In most of the world, spent nuclear fuel is placed in dry casks after several years of cool down in water pools. The plutonium in the spent nuclear fuel can be chemically separated. The proliferation risk is currently dealt with by carefully tracking the loading and storage of the casks and by using seals to ensure that there has been no tampering between periodic inspections.

Three decades of effort have been spent searching for methods to make passive gamma ray or neutron measurements that can physically determine if the fuel in a cask has been tampered with. The shielding provided by the cask walls has largely thwarted these efforts [1,2]. A number of groups have used models to examine the possibility of using muon tomography [3] to non-destructively inspect nuclear fuel in dry cask storage [4–10]. Recent data obtained on a partially loaded Westinghouse model MC-10 dry cask at Idaho National laboratory have been used to demonstrate that muon tomography provides a method than can detect missing fuel bundles [11–13] using data taken with the Los Alamos mini-muon tracker [14].

These results have been extended using a validated GEANT-4 [15] model to estimate the counting times and data quality that could be obtained with a better-suited detector [16,17]. This modelling has shown that it is possible to find missing fuel bundles with time exposures of days.

In this paper, we apply the techniques used in [11,12,16,17] to examine the signatures of diversion of spent fuel that can be detected using muon tomography.

2. Techniques

E. P. George was the first to use cosmic ray muons as a radiographic tool [18]. Others followed this work, which relied on the long path length of muons (approx. $1\,\mathrm{kg\,cm^{-2}}$) to radiograph thick geological and archaeological features. The range over which muon radiography could be applied was extended to much thinner objects by the work of Borozdin *et al*. [3], where it is shown that the Coulomb scattering of muons could be used for radiography. The transmission and stopping of muons depend upon the electron density of the materials the muons are traversing. The energy loss of muons traversing material is given by the Bethe–Block equation:

$$\frac{\mathrm{d}E}{\mathrm{d}x} = Kz^2\frac{Z}{A}\frac{1}{\beta^2}\left[\frac{1}{2}\ln\left(\frac{2m_e c^2\beta^2\gamma^2 T_{\max}}{I^2}\right) - \beta^2 - \frac{\delta(\beta\gamma)}{2}\right], \tag{2.1}$$

where Z and A are the atomic charge and atomic number of the material, respectively, β is the muon velocity divided by of the speed of light, c, $\gamma = 1/\sqrt{1-\beta^2}$, I is the average ionization potential of the material, $T_{\max}$ is the maximum energy that can be transferred to an electron in a single collision, and K is a constant. As muons lose all of their energy and stop they are removed from the incident flux. The attenuation of muons provides a radiographic tool.

Coulomb scattering through a slab of material of thickness L is approximately described by a Gaussian shaped angular distribution, $\mathrm{d}N/\mathrm{d}\theta$, the Fermi approximation:

$$\frac{\mathrm{d}N}{\mathrm{d}\theta} = \frac{1}{2\pi\theta_0^2}\mathrm{e}^{-\frac{\theta^2}{2\theta_0^2}}\,\mathrm{d}\Omega, \tag{2.2}$$

Where the width, θ_0, is given by

$$\theta_0 = \frac{14.1}{p\beta}\sqrt{\frac{L}{X_0}}, \tag{2.3}$$

where p is the muon momentum in units of MeV/c, L is the thickness of the object and

$$X_0 = \frac{K}{A}\{Z^2[L_{\mathrm{rad}} - f(Z)] + ZL'_{\mathrm{rad}}\}, \tag{2.4}$$

where $f(Z)$ is a slowly varying function of Z, K, L_{rad} and L'_{rad} are slowly varying functions of Z.

The summations/integrals for objects composed of mixed materials are straightforward.

Scattering radiography is accomplished by measuring the trajectories of both incoming and outgoing muons in a set of position sensitive tracking detectors. Scattering information for the ith trajectory is obtained using the incident, $\boldsymbol{v}_{\text{in},i}(x, y, z_{\text{in}}, x', y', z')$, and outgoing, $\boldsymbol{v}_{\text{out},i}(x, y, z_{\text{out}}, x', y', z')$ muon directions using the tracking detectors and the scattering angle can be calculated as

$$\theta_{\text{scatt},i} = \arccos(\boldsymbol{v}_{\text{in},i} \cdot \boldsymbol{v}_{\text{out},i}). \tag{2.5}$$

Stopping/transmission is also obtained using both the incident and outgoing trajectories. Being able to identify both transmitted and stopped tracks (no outgoing information) provides a statistical advantage over measuring only the transmitted tracks.

Positions were calculated using the incident trajectories for both scattering and transmission radiography. We calculate the points of closest approach between the incident trajectory, $\boldsymbol{v}_{\text{in},i}$, and the fuel cask axis, $\boldsymbol{a}$, $p_{2,i}(x, y, z)$ and $p_{1,i}(x, y, z)$, respectively. The quantity $d_i = \text{sgn}(\boldsymbol{t}_i \times \boldsymbol{p}_i \cdot \boldsymbol{a})||\boldsymbol{p}_i||$, where $\boldsymbol{p}_i = (p_{2,i}(x, y, z), p_{1,i}(x, y, z))$, forms one axis of a sinogram that can be used for two-dimensional analysis of the fuel cask contents for both scattering and transmission radiography. The other axis is the angle of incident trajectory in the plane orthogonal to the cask. The values are either the number of radiation lengths (see below) from the scattering angles or the negative logarithm of the transmission, summed over the index i, for scattering and transmission analysis, respectively. For this analysis, the distances were binned in 2.0 cm steps and the angles were binned in 2-degree steps.

To first order, energy loss is proportional to the electron density, Z/A, whereas multiple scattering is proportional to Z^2/A. Measuring both scattering and transmission allows a separation of the average charge and the material density and can provide material identification [19].

3. Spent nuclear reactor fuel

Power is generated in nuclear reactors by fissioning predominantly the ^{235}U and ^{239}Pu. The ^{239}Pu is created by neutron capture on ^{238}U as the ^{235}U burns. Although the fission process conserves the charge of the initial nucleus it divides it between the two fission product nuclei. The electron density in the fuel remains constant to first order while the average charge decreases.

The plutonium in spent nuclear fuel is a proliferation risk, because it can be separated chemically from the other materials. This process becomes easier as the fuel ages and its specific activity decreases.

Licensing of permanent repositories for spent fuel has been slow worldwide. Currently, much of the inventory of spent fuel is stored in dry shielding casks. Generally, these are sealed and placed under video surveillance to prevent diversion of the fuel. There have been three decades of research devoted to finding methods that can be used to restore confidence in the integrity of the stored fuel in anticipation of the potential loss of the continuity of knowledge (CoK) of the seals and surveillance in cases of human-created or natural disasters [1,2].

In commercial reactors, the amount of heavy metal that is lost to fission is characterized by the burnup fraction. Burnup is given either in units of per cent or in more easily measured gigawatt days per ton (GWd/T) of energy extracted from the fuel. These two measures are approximately proportional to each other.

Figure 1 shows the ^{239}Pu content of a fuel bundle as a function of burnup. Four fuel bundles are required to obtain 8 kg of ^{239}Pu, the so-called IAEA significant quantity (SQ) [20].

Recent work [21] provides a detailed inventory of the nuclear products of spent fuel as a function of burnup, generated using the code Monteburns which links the Monte Carlo transport code MCNP to isotope generation and depletion tools such as CINDER or ORIGEN to provide both time- and energy-dependent system parameters. The 1/8th core model representing a Pressurized Water Reactor throughout different irradiation cycles provided isotopic compositions on a per pin basis for the simulated fuel assemblies examined in this research for a number of variety of burnups, initial enrichments and cooling times.

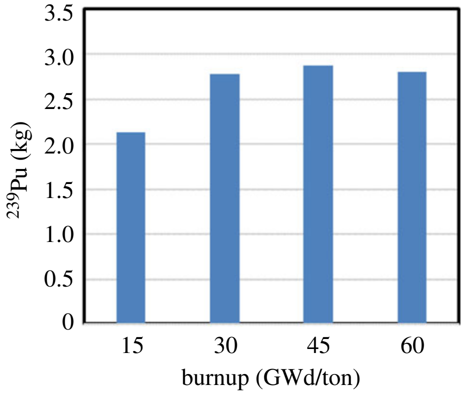

Figure 1. ^{239}Pu content of a fuel bundle as a function burnup. (Online version in colour.)

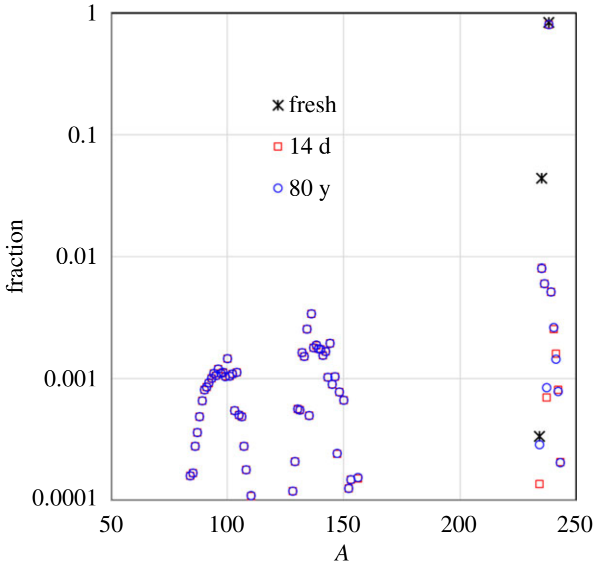

Figure 2. Effect of burnup on isotopic composition of fuel. The small change in the isotope distribution as a function of time of storage can be seen in the difference between the red and blue curves. (Online version in colour.)

The isotope distributions for fresh fuel (x's) and fuel with a burnup of 60 GW days/ton of heavy metal (red and blue circles) are shown in figure 2. The double-humped distribution of the fission products is apparent. The burnup fraction at this exposure is 5.5%. In the simplest model, where the atomic number of the fission products is half of the starting nuclei, the scattering is expected to be reduced by approximately 2.5% because of the burnup while the transmission should remain the same when the burned fuel is compared to fresh fuel. The similarity of the 14-day and 80-year isotope distributions shows there are only small changes due to β-decay.

The resulting fuel compositions have been incorporated into a GEANT-4 [15] model of a TN-24P fuel cask [22] in order to study the signatures of fresh and spent fuel, the impact of β-decay on muon scattering of spent fuel, and the change in the signature from various materials that could be used to replace diverted fuel bundles.

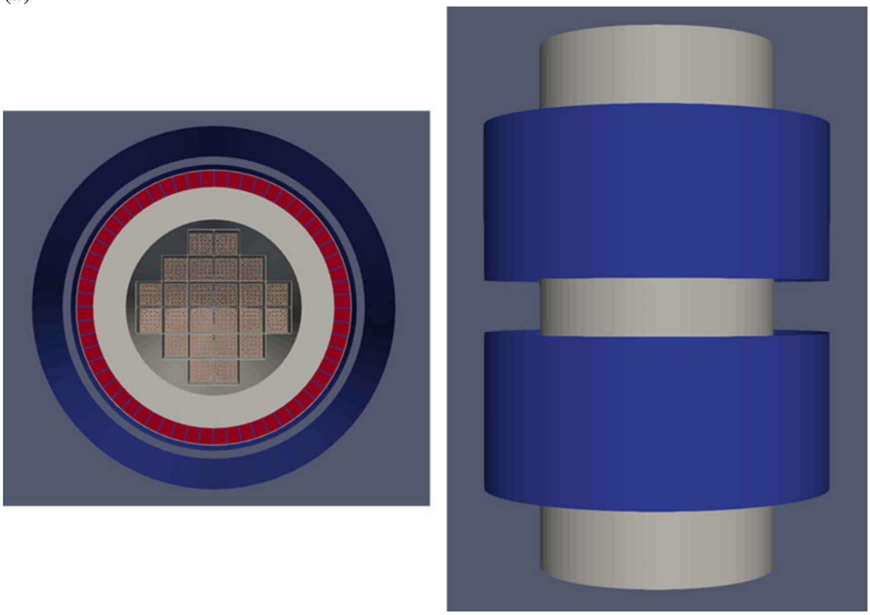

Figure 3. (*a*) Top view and (*b*) side view of the geometry used to model muon radiography of a fuel cask. (Online version in colour.)

4. Fuel cask model

The description for the Geant4 [15] model of the TN-24P storage cask was taken from [22]. The cask consists of a 270 mm thick steel shell for gamma shielding surrounded by an outer shell with 60 copper cooling fins that run the length of the steel shell, have a width of 11.4 mm, and protrude radially from the shell 133 mm. The volume between the fins is filled with a boron-loaded resin for neutron shielding. The resin is modelled as a generic borated polyethylene because composition details were unavailable. A 10 mm steel skin wraps around the outside of the cask. The cask interior contains interlocking aluminium plates, 10 mm thick, that create a containment basket to hold the spent fuel bundles. All components of the cask run above the upper muon detector and below the lower muon detector to create a uniform distribution in the vertical direction within the detector's field of view.

The detectors were modelled as two 150 cm high cylindrical shells with radii of 168 cm centred on the cask axis. There was a 50 cm gap between the detectors. Each detector was ideal in tracking and position, i.e. the detector resolution was not considered in this study due to the large multiple Coulomb scattering within the cask, which would obscure any reasonable detector uncertainty in angle and position. A schematic view of this model is shown in figure 3.

5. Tomographic algorithm

Although a full 3-d tomographic model of a fuel cask could be obtained with long enough exposure, we assume that it is unlikely that partial fuel rods would be loaded into the cask in diversion scenarios. Whole fuel bundles will most probably be removed, and may be replaced with surrogate materials to avoid detection. This allows the tomographic problem to be reduced to a single slice averaged over the direction along the fuel bundles (the cask axis).

For the scattering analysis, a three-dimensional histogram was formed. The scattering angles were histogrammed for each bin of the scattering sinogram in the in 2 mrad steps. The resulting angular distributions were fitted with a modified multi-group model. The multi-group model

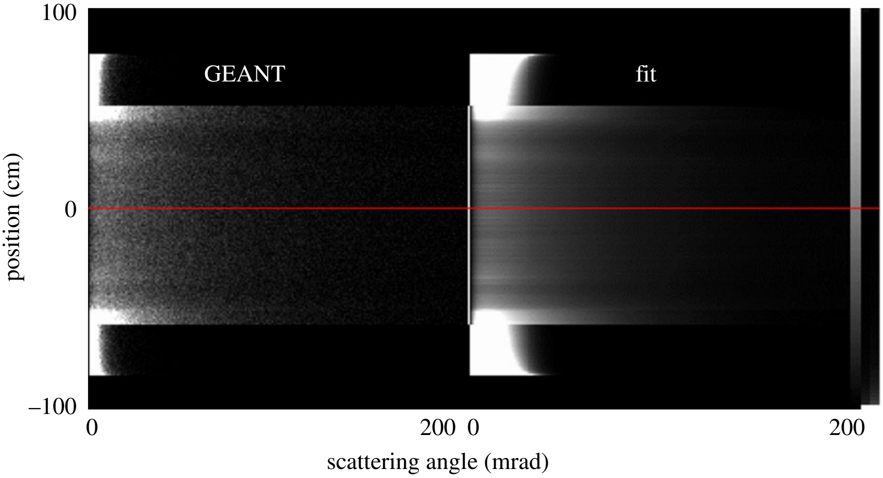

Figure 4. Scattering angle distribution, θ_{scatt}, for a single 2° slice from the angular scattering sinogram data. (Online version in colour.)

described in references [19,23,24] uses a multi-group model of the cosmic ray muon energy spectrum to fit the measured angular distribution. Unlike other methods, this provides a good description of the tails in the angular distribution and provides more precise thickness precision [25].

The muon momentum distribution, $\mathrm{d}N/\mathrm{d}\theta$, is given by

$$\left.\begin{aligned}
\frac{\mathrm{d}N}{\mathrm{d}\theta} &= N\sum_i \frac{A_i(p_i-\Delta p)}{p_i-\Delta p}\,\mathrm{e}^{-\frac{\theta^2}{2\sigma_0^2}}, \\
\sigma_i(t) &= \frac{14.1}{p_i-\Delta p}\sqrt{t}, \\
\Delta p &= \frac{\mathrm{d}p}{\mathrm{d}t}t, \\
A_i(p_i-\Delta p) &= 0 && \text{if } p_i-\Delta p<0, \\
&= \frac{p_i-\Delta p}{p_i}A_i(p_i) && \text{if } p_{i-i}-\Delta p<0, \\
&= A_i(p_i) && \text{otherwise,}
\end{aligned}\right\} \tag{5.1}$$

where t is the thickness measured in radiation lengths, p is the muon momentum in units of MeV/c, $\mathrm{d}p/\mathrm{d}t$ is the momentum loss per radiation length which has been taken as constant in this work, and N is a normalization factor that is adjusted to ensure the integral is 1. The thickness, t, is fitted to the angular distribution for each pixel in the sonogram assuming Poisson statistics by the maximum-likelihood method using a simple fitting algorithm. The fit used a simple grid search with one quadratic iteration to interpolate to the minimum.

The parameters, A_i, were obtained by fitting high statistics data from a simulation of just an empty steel shell using equation (5.1). The expected difference in $\mathrm{d}p/\mathrm{d}t$ for the different materials was not considered.

An example of the angular distributions for one angle slice from the simulation is shown in figure 4. On the left is the data from the simulation and on the right is the fit. A line plots taken at one position, shown by the red line, through the data and fit are shown in figure 5. One can see the shape of the angular distribution is well fitted by the model.

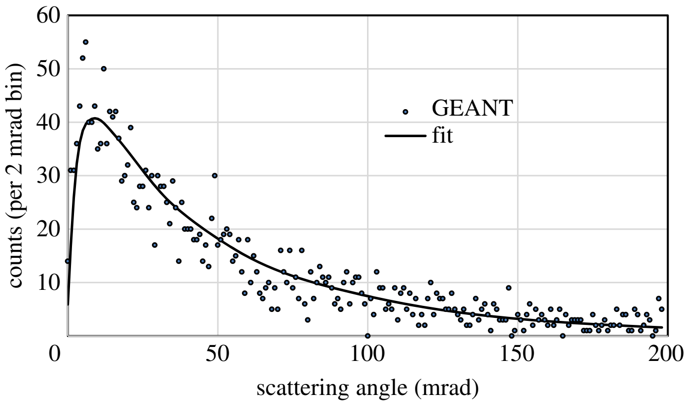

Figure 5. Single line plot of θ_{scatt} taken along the red line in figure 4.

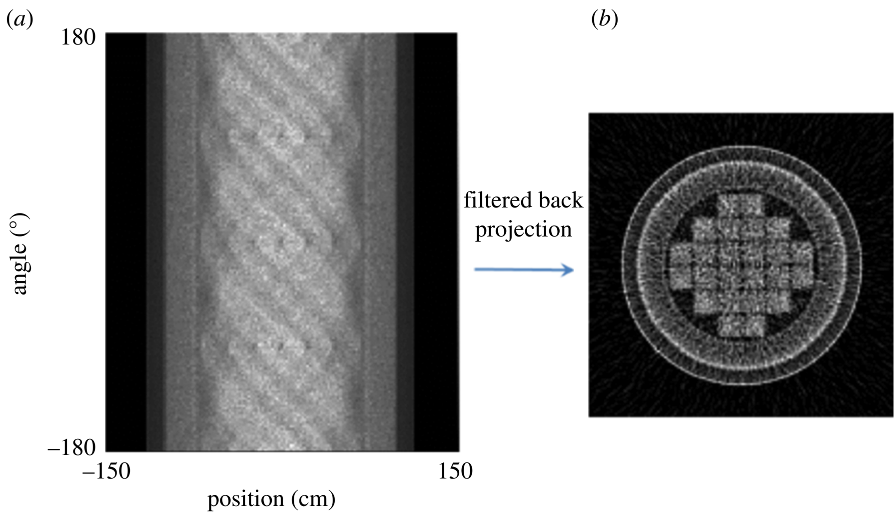

Figure 6. (*b*) Sinogram (*a*) volume density plot after applying filtered back projection. (Online version in colour.)

A sinogram obtained from the simulation of spent fuel and the result of applying filter back projection, to obtain a tomographic slice, are shown in figure 6. The image clearly shows each of the individual fuel bundles.

For transmission, separate histograms were stored for all incident and transmitted trajectories. A sinogram was created by calculating the negative logarithm of the ratio of these. The implicit assumption is that the stopping rate is constant independent of thickness. This assumption greatly simplifies the analysis and appears to be justified by the results which give approximately the correct and constant densities for the steel and fuel in filter back projection reconstructions.

6. Results

We have performed simulations of 8×10^7 muons (approx. 7 days of exposure) and have analysed the results to determine the sensitivity of muon scattering and stopping tomography to various diversion scenarios. We have analysed both the scattering and stopping signals. For the simplest analysis, we formed the sinograms for the loaded and empty cask, subtracted the empty from the loaded sinogram, integrated the difference and plotted this signal for each of the scenarios

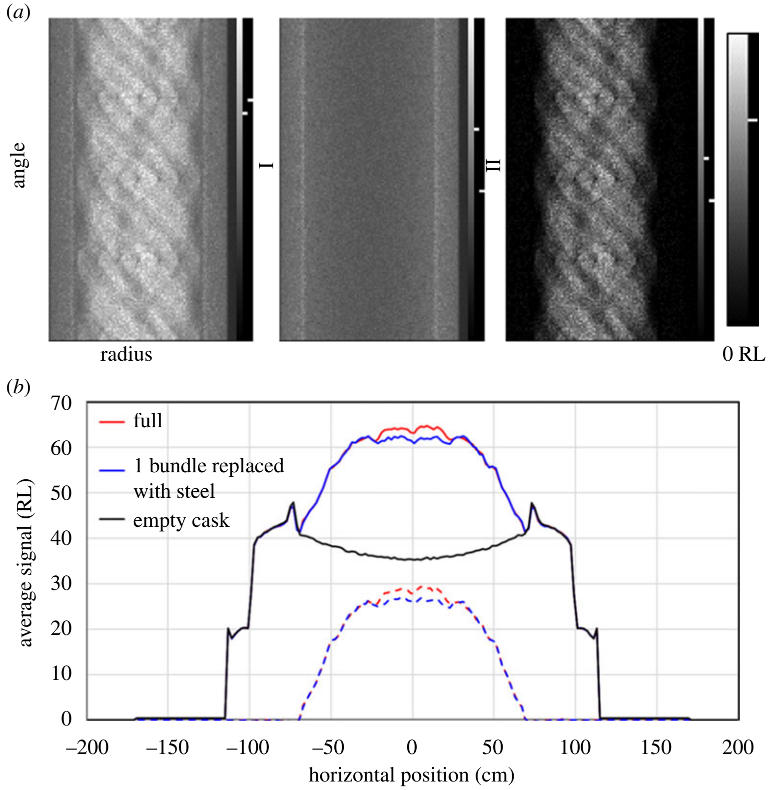

Figure 7. (*a*) images of the sinograms for a loaded, empty, and the difference for a cask where one bundle has been replaced by steel. (*b*) Plots of each of the sinograms averaged over angle. (Online version in colour.)

studied. An example with one fuel bundle replaced with steel is shown in figure 7. The effect from the steel bundle is clearly observed in the sinograms and in the average signal comparison shown in the plot.

We have compared a cask with fresh fuel and spent fuel with about 5.5% burnup, spent fuel stored for 0, 40 and 80 years, and a cask with one of the inner fuel bundles missing or replaced with fresh fuel, steel, lead (Pb) or depleted uranium (DU). The average signal for each of the simulations is plotted in figure 8. The error bars reflect only statistical errors.

The difference between the scattering signal for fresh and spent fuel is 2.5% and the uncertainties are about 0.1%. As expected there is no detectable difference in the stopping signal, which has an uncertainty of approximately 0.4%. This suggests that in principle it is possible to fingerprint fuel casks by measuring the burnup of the fuel *in situ*. Such measurements could most precisely be accomplished differentially, i.e. by comparing measurements across events where CoK has been lost. Achieving 0.1% precision would require careful control for atmospheric pressure, detector efficiency and geometry and all other potential variables. Further research is needed to establish the level of precision that can be obtained. Missing and replaced fuel bundles are readily apparent in this average signal except for the cases of DU and fresh fuel. At 0.1% precision, the replacement of approximately 4 bundles (1 SQ) should be detectable in the average signal which is 24 standard deviations if all of the bundles are replaced.

A more sensitive test of diverted fuel bundles can be obtained by applying tomography to the sinograms. We have applied a model fitting algorithm. The model used is defined by the densities of a hollow cylinder to model the body of the cask, a cylinder with the inside radius of the cask to model the material in the inner structure of the cask, and 24 densities, one for each fuel bundle.

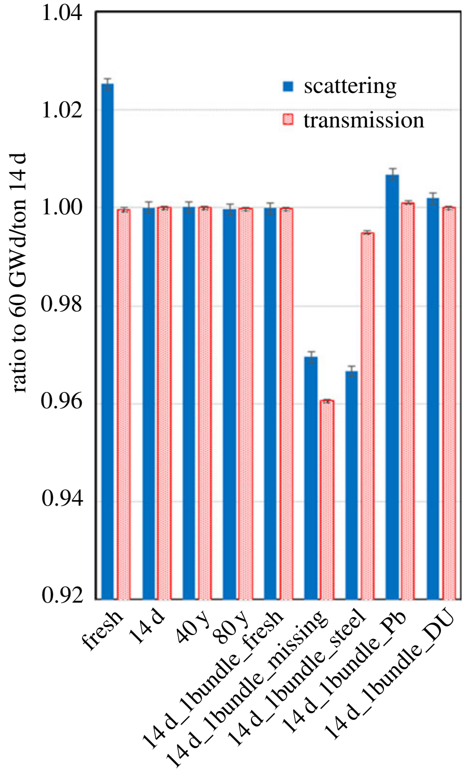

Figure 8. Ratio of the averaged sinogram signals between the diversion scenarios and a fully loaded cask for scattering (blue/solid) and transmission (red/shaded) radiography. (Online version in colour.)

This gives 26 densities, a_i. The model is solved by fitting to the sinogram using linear least squares. If the areal density in an element of the sinogram is given by ρ_k, then

$$\rho_k = \sum_i p_{ki} a_i. \tag{6.1}$$

One can form an X^2 as

$$X^2 = \sum_k \left(\sum_i p_{ki} a_j - y_k \right)^2 \tag{6.2}$$

where y_k is the measured sinogram. The index k runs over both angles and position in the sinogram. The a's are found by solving:

$$\frac{\mathrm{d}X^2}{\mathrm{d}a_j} = 0 = \sum_k 2 \left(\sum_i p_{ki} a_j - y_k \right) p_{kj}, \tag{6.3}$$

The sums can be interchanged resulting in the matrix equation:

$$\mathbf{AM} = \mathbf{Y}, \quad \text{where } \mathbf{A} = a_i, \mathbf{Y} = \sum_k y_k p_{kj}, \mathbf{M} = \sum_k p_{kj} p_{ki}. \tag{6.4}$$

The solution,

$$\mathbf{A} = \mathbf{M}^{-1}\mathbf{Y}, \tag{6.5}$$

can be found by matrix inversion.

The resulting densities from the fits to the sinograms are shown in figure 9. Deficiencies in the model are apparent in the consistent variation in the fuel bundle densities as a function

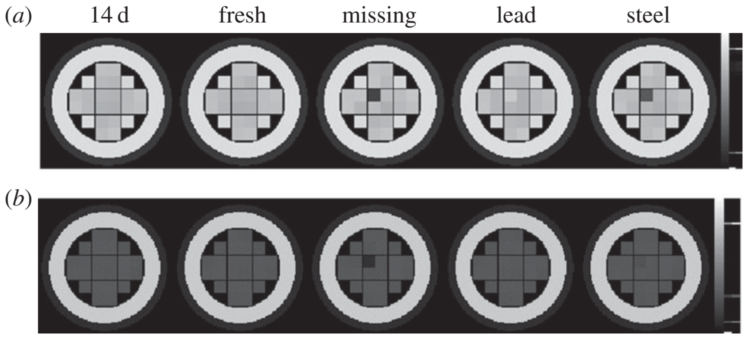

Figure 9. Tomographic volume densities obtained for scattering (*a*) and transmission (*b*) tomography for a fully loaded cask (left) and four cases where a full bundle has been removed and either left empty or replaced.

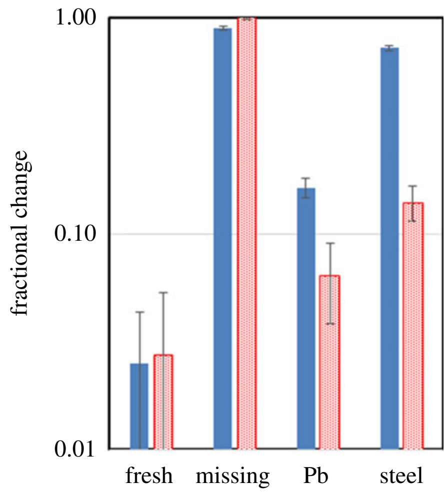

Figure 10. Absolute value of factional change of the density signal in the missing bundle slot between four diversion scenarios shown in figure 9 and the fully loaded cask for scattering (blue/solid) and transmission (red/shaded) radiography. (Online version in colour.)

of position. A more complete model would improve this. Nevertheless the fuel bundle that is missing, replaced with lead, or replaced with steel is easily identified in the images.

The absolute value for the fractional changes of the densities for the missing fuel bundles obtained from this analysis is plotted in figure 9. Although a single fresh fuel bundle is difficult to detect, the missing lead and steel replacement fuel bundles are observed with high likelihood in both the scattering and transmission imaging. It is clear that scattering gives a more significant signal for the lead and steel fuel bundles whereas the transmission signal is more significant for the missing fuel bundle.

Although either scattering or transmission could be spoofed by making dimensional changes to match the scattering or transmission of the fuel, it is not possible to match both simultaneously easily because of the unique mix of uranium and fission products specific to the loaded fuel.

The absolute value of the fractional change of the fitted density between the diversion scenario and the spent fuel is plotted in figure 10. Numerical results are given in table 1. The value of the scatter signal when compared to the transmission signal is apparent. It is also clear that most of the diversion scenarios considered here can be detected with considerably less precision, allowing for shorter exposure times and less precise data.

Table 1. The signals and significance in standard deviations (s.d.) of the data plotted in figure 10.

	scatter			transmission		
	signal	Δsignal	s.d.	signal	Δsignal	s.d.
fresh	0.03	0.01	1.67	0.03	0.03	1.06
missing	0.90	0.01	60.24	1.01	0.03	39.23
Pb	0.16	0.01	10.95	0.06	0.03	2.48
steel	0.73	0.01	48.49	0.14	0.03	5.41

7. Conclusion

We have presented a numerical study of scattering and transmission cosmic ray radiography/tomography with the goal of fingerprinting spent fuel casks. We have shown that there is a 2.5% difference between the scattering signals from fresh and spent fuel with 5.5% burnup (60 GW days/ton of heavy metal). One week of muon exposure with two 1.5 m high detectors that surround the cask is sufficient to measure the scattering signal to 0.1% precision. This precision is sufficient to detect the diversion of a single bundle of fuel either removed or replaced with a common material such as lead or iron. Although the signal from a single bundle replaced with fresh fuel or DU is too small to be reliably detected at this precision, the replacement of four bundles, enough to obtain 1 SQ of Pu, would give a 4 s.d. signal.

Data accessibility. The data are included as an excel spreadsheet in the electronic supplementary material.

Authors' contributions. D.P. performed simulations and analysis. J.B. contributed to defining potential detector geometries and contributed to data acquisition. M.D., E.G. and C.L.M. contributed to the muon analysis algorithms, intellectual input and data acquisition. H.R.T. provided spent fuel descriptions. All authors contributed to the ideas, writing and editing the paper.

Competing interests. Authors declare that they have no competing interests.

Funding. We acknowledge the support of the Los Alamos Laboratory Research and Development for this work.

References

1. Ziock K-P, Caffrey G, Lebrun A, Forman L, Vanier P, Wharton J (eds). 2005 Radiation imaging of dry-storage casks for nuclear fuel. In *Nuclear Science Symp. Conf. Record*, 23–29 Oct. 2005, Fajardo, Puerto Rico: IEEE. (doi:10.1109/NSSMIC.2005.1596457)
2. Peerani P, Galletta M. 2007 Re-establishment of the continuity of knowledge in the safeguards of interim storages using NDA techniques. *Nucl. Eng. Des.* **237**, 94–99. (doi:10.1016/j.nucengdes.2006.04.001)
3. Borozdin KN, Hogan GE, Morris C, Priedhorsky WC, Saunders A, Schultz LJ, Teasdale ME. 2003 Surveillance: radiographic imaging with cosmic-ray muons. *Nature* **422**, 277. (doi:10.1038/422277a)
4. Chatzidakis S. 2017 *Classification and imaging of spent nuclear fuel Dry casks using cosmic ray muons*. Oak Ridge, TN: Oak Ridge National Laboratory (ORNL).
5. Chatzidakis S, Choi C, Tsoukalas L. 2016 Interaction of cosmic ray muons with spent nuclear fuel dry casks and determination of lower detection limit. *Nucl. Instrum. Methods Phys. Res.* **828**, 37–45. (doi:10.1016/j.nima.2016.03.084)
6. Chatzidakis S, Choi CK, Tsoukalas LH. 2016 Analysis of spent nuclear fuel imaging using multiple coulomb scattering of cosmic muons. *IEEE Trans. Nucl. Sci.* **63**, 2866–2874. (doi:10.1109/TNS.2016.2618009)
7. Chatzidakis S *et al.* 2017 *Exploring the use of muon momentum for detection of nuclear material within shielded spent nuclear fuel dry casks*. Oak Ridge, TN: Oak Ridge National Laboratory (ORNL).
8. Jonkmans G, Anghel V, Jewett C, Thompson M. 2013 Nuclear waste imaging and spent fuel verification by muon tomography. *Ann. Nucl. Eng.* **53**, 267–273. (doi:10.1016/j.anucene.2012.09.011)

9. Jonkmans G, Anghel VNP, Thompson M. 2010 Muon tomography for imaging nuclear waste and spent fuel verification. Atoms for Power, Health and the Environment 31st annual conference of the Canadian Nuclear Society and 34th annual conference of the Canadian Nuclear Society and Canadian Nuclear Association, (p. 111 Megabytes). Canada: Canadian Nuclear Society.
10. Tsoukalas LH. 2016 *Creation of a Geant4 muon tomography package for imaging of nuclear fuel in dry cask storage*. West Lafayette, IN: Purdue University.
11. Durham J *et al.* 2018 Verification of spent nuclear fuel in sealed dry storage casks via measurements of cosmic-ray muon scattering. *Phys. Rev. Appl.* **9**, 044013. (doi:10.1103/PhysRevApplied.9.044013)
12. Durham JM *et al.* 2016 Cosmic ray muon imaging of spent nuclear fuel in dry storage casks. *J. Nucl. Mater. Manag.* **44**, 5.
13. Guardincerri E *et al.* (eds). 2015 Cosmic-ray imaging of spent fuel casks. In *APS Division of Nuclear Physics Meeting Abstracts*, APS Division Nuclear Physics Sante Fe Meeting 2015. APS.
14. Perry J. 2013 *Advanced applications of cosmic-ray muon radiography*. The University of New Mexico. (https://digitalrepository.unm.edu/ne_etds/4)
15. Agostinelli S *et al.* 2003 GEANT4—a simulation toolkit. *Nucl. Instrum. Methods Phys. Res.* **506**, 250–303. (doi:10.1016/S0168-9002(03)01368-8)
16. Poulson D, Durham JM, Guardincerri E, Morris C, Bacon J, Plaud-Ramos K, Morley D, Hecht AA. 2017 Cosmic ray muon computed tomography of spent nuclear fuel in dry storage casks. *Nucl. Instrum. Methods Phys. Res.* **842**, 48–53. (doi:10.1016/j.nima.2016.10.040)
17. Poulson DC *et al.* 2017 Application of filtered back projection to muon radiography for imaging dry storage casks. *Nucl. Instrum. Methods Phys. Res.* **842**, 48–53.
18. George EP. 1955 Cosmic rays measure overburden of tunnel. *Commonwealth Engineer.* July 1 1955, pp. 455–457.
19. Morris CL *et al.* 2012 Obtaining material identification with cosmic ray radiography. *AIP Adv.* **2**, 042128. (doi:10.1063/1.4766179)
20. IAEAI. 2002 *Safeguards glossary, 2001 edition*. *International nuclear verification series*, vol. 3, 23. Vienna, Austria: International Atomic Energy Agency.
21. Trellue HR, Galloway JD, Fischer NA, Tobin SJ (eds). 2013 Design and Description of the NGSI Spent Fuel Library with Emphasis on the Passive Gamma Signal. *J. Nucl. Mater. Manag.* **40**, 25.
22. McKinnon MA, Michener TE, Jensen MF, Rodman GR. 1989 Testing and analyses of the TN-24P PWR spent-fuel dry storage cask loaded with consolidated fuel. United States: N. p. (doi:10.2172/6372210)
23. Morris C *et al.* 2013 A new method for imaging nuclear threats using cosmic ray muons. *AIP Adv.* **3**, 082128. (doi:10.1063/1.4820349)
24. Morris CL *et al.* 2014 Horizontal cosmic ray muon radiography for imaging nuclear threats. *Nucl. Instrum. Methods Phys. Res., Sect. B.* **330**, 42–46. (doi:10.1016/j.nimb.2014.03.017)
25. Perry JO, Bacon J, Borozdin K, Fabritius J, Morris C. 2014 Analysis of the multigroup model for muon tomography based threat detection. *J. Appl. Phys.* **115**, 064904. (doi:10.1063/1.4865169)